scientific reports

OPEN

Effect of fabrication error on the sensitivity of a one-dimensional photonic crystal sensor for cancer detection

Ali Mohammadi, Seyed Asghar Mohammadi & Mehdi Hosseini✉

One-dimensional photonic crystal (1D-PC) biosensors are promising for applications like cancer detection due to their high sensitivity, but their performance is often compromised by unavoidable fabrication errors. However, theoretical analyses often do not quantitatively assess the impact of these fabrication errors on key sensor performance parameters, such as sensitivity and peak width. This study addresses this issue by performing a statistical analysis to investigate how random fabrication deviations influence these performance metrics, thereby providing a more realistic evaluation of sensor stability and robustness. For a designed 1D-PC biosensor, the transmission spectrum was first calculated using the transfer matrix method (TMM). A statistical simulation was then performed to analyze how random errors in layer thickness affect the sensor's performance at various error levels (δ) and at two incidence angles, 0° and 85°, with 100 iterations per level. The results showed that as fabrication errors increase, the values for the transmission peak position and Full Width at Half Maximum (FWHM) deviate from their ideal, error-free state. The sensitivity also fluctuates around the ideal value. Interestingly, it was found that some sensor instances could achieve sensitivities higher than the ideal, error-free value. The findings confirm that the 85° incidence angle, previously optimized[1] for high sensitivity, also provides enhanced resistance to fabrication errors compared to normal incidence, making it a robust choice for practical applications and guiding the design of more stable biosensors.

Keywords Photonic crystal, Biosensor, Cancer detection, Fabrication error, Sensitivity

The early detection of cancer is a primary challenge in modern medicine, as the success of treatment is highly dependent on the stage of diagnosis[1–3]. Current cancer detection methods, like biopsy and imaging, are often invasive, time-consuming, and costly[4–6]. Therefore, developing non-invasive, rapid, and cost-effective methods for cancer detection is highly important[2,7–9]. In response to this need, significant advancements have been made in developing novel optical and nanophotonic sensor platforms for medical applications. These advancements include nanophotonic photoacoustic (PAS) sensors for real-time monitoring of cancer therapy[10], smart optical sensor-based catheters for minimally invasive biosensing[11], and nanostructured probes for neurotherapeutic applications[12]. Furthermore, nanomaterial-based biosensors, such as electrochemical sensors, have offered promising solutions for the rapid detection of pathogens (like zoonotic diseases)[13,14], and novel nanostructured materials have been synthesized for antibacterial applications. Moreover, the convergence of these sensors with artificial intelligence (AI) has opened new horizons in precise diagnostics; from using deep learning for automated analysis of microscopy (TEM) images to supporting clinical decision-making in 5th/6th generation smart sensors[5,15]. Among these emerging technologies, biosensors based on PCs have attracted special attention for cancer detection applications due to their high sensitivity and integration capabilities[6]. 1D-PCs are well-known for their multilayered structures and their light-filtering capabilities[16–20]. Due to their ability to control and manipulate light within specific wavelength ranges, these structures have found extensive applications in various fields, including biosensors, optical filters, and solar cells[1,21–25]. These structures can detect the presence of specific biomolecules by altering their optical properties, such as changes in reflectivity or light absorption[26–29]. Moreover, PC sensors are prominent candidates for sensing applications, as they offer simple integration with optical integrated circuits (OICs), a compact size, high operational speed, and considerable precision[30–34]. The operating principle of this sensor is based on the PBG phenomenon. The crystal's periodic structure acts as an

Department of Physics, Shiraz University of Technology, Shiraz, Iran. ✉email: hosseini@sutech.ac.ir

optical filter, preventing the transmission of a wide range of wavelengths[35,36]. However, introducing a defect layer into the center of the structure breaks this periodic symmetry. This leads to the creation of an allowed state within the PBG, known as a "defect mode." This mode appears in the structure's transmission spectrum as a very narrow and sharp resonance peak at a specific wavelength (λ_{res}). When a biological sample enters the defect layer, it alters the layer's effective refractive index. This change, however small, causes a shift in the spectral position of the defect mode ($\Delta\lambda_{res}$)[7–41,43–46,48,59,61]. This spectral shift constitutes the sensor's output signal, and by precisely measuring it, the presence or concentration of the analyte can be determined. The primary metric for the quantitative evaluation of this performance is the sensor's sensitivity (s), defined in Eq. 1, as the ratio of the resonance wavelength shift to the change in the refractive index of the defect layer:

$$s = \frac{\Delta\lambda_{res}}{\Delta n_{res}} \tag{1}$$

Various methods are used to fabricate 1D-PCs, such as evaporation[16,42], sputtering[18,47], and dip/spin coating techniques[17,49]. Anodic etching of crystalline silicon is another method used for creating these crystals[50–53]. These crystals are also fabricated using low-pressure chemical vapor deposition[19]. The early detection of cancer is a primary challenge in modern medicine, as the success of treatment is highly dependent on the stage of diagnosis. Current cancer detection methods, like biopsy and imaging, are often invasive, time-consuming, and costly. Therefore, developing non-invasive, rapid, and cost-effective methods for disease detection is highly important. Given the layered nature of PCs and the fabrication methods described above, a certain degree of error in the thickness of each layer is always present[54–56]. These fabrication imperfections, also known in the literature as "disorder," represent a fundamental and ubiquitous challenge in nanophotonic devices[55,57]. Extensive research has shown that these errors, even on very small scales (on the order of nanometers), can have detrimental effects on the performance of various photonic crystal devices[58]. For example, random errors in the position or radius of holes can lead to severe scattering losses, a significant reduction of the quality factor (Q-factor) in cavities, and unpredictable shifts in the resonance wavelength[58,59]. These tolerances are so critical that they can cause the complete failure of filters or logic gates and make the fabrication of arrays of identical devices virtually impossible[58,60]. These challenges are particularly significant for sensors, as their operation relies directly on the precise measurement of these small resonance wavelength shifts[61]. Therefore, a quantitative and statistical understanding of these errors is crucial for evaluating the robustness and reliability of sensors before committing to costly fabrication[61]. The abnormal refractive index of cell cytoplasm caused by cancer[62–65] is a crucial biomarker for cancer diagnosis, which can be utilized to construct a sensor for detecting cancer cells[66].

The thickness of thin films, particularly in plasmonic or photonic regions, plays a vital role in determining the sensor's sensitivity; sensitivity increases with thickness up to a certain limit and subsequently decreases[67]. In this study, the sensor structure and its design parameters are adapted from the work conducted by Aly and Zaky in 2019[1]. That foundational study introduced a high-sensitivity photonic crystal sensor (2156 nm/RIU at an 85° incidence angle) under ideal, error-free fabrication conditions. However, a critical research gap remains: the lack of a quantitative assessment of the stability of this optimized sensitivity against the statistical effects of real fabrication errors. While previous research has primarily focused on inherently error-tolerant designs or on evaluating errors in different sensor types[54,68], the key differentiation of the present work is its focus on fabrication errors in layer thickness and the specific investigation of how these deviations impact the sensor's performance. The aim of this work is to systematically analyze the effect of minor manufacturing process deviations on various PC sensor parameters to determine whether the 85° angle, selected for maximum sensitivity, also offers superior robustness against fabrication errors, which is paramount for practical applications.

Methods

The sensor structure under investigation is a 1D-PC. As shown in Fig. 1, it consists of five periodic units ($N = 5$) made of dielectric bilayers: silicon dioxide (SiO_2) with a refractive index of $n_1 = 1.44$ and gallium arsenide (GaAs) with a refractive index of $n_2 = 3.36$.[1] These materials were chosen due to their high refractive index contrast, which is essential for creating a wide and well-defined photonic bandgap (PBG), and their low absorption in the operating wavelength range[1].

Under ideal design conditions, the thicknesses of these layers are set to d_1=260.42 nm and d_2=111.61 nm, respectively. A defect layer, or cavity, with a refractive index n_d and thickness $13d_d$ is embedded in the center of this periodic structure, which serves as the slot for the biological sample. The thickness of the defect layer, d_d, is

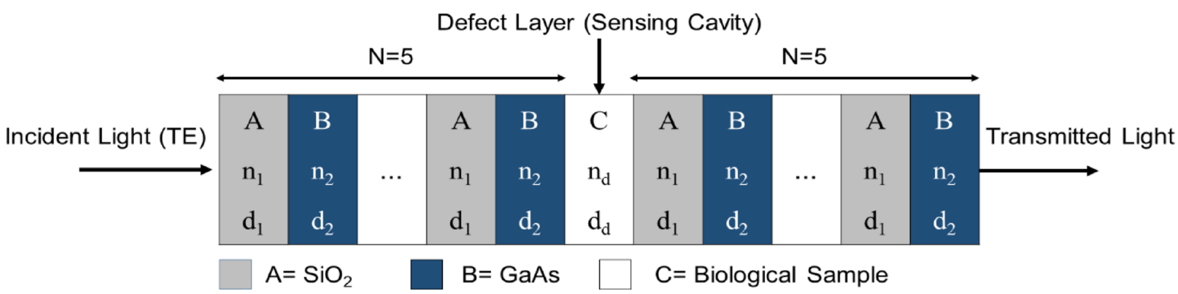

Fig. 1. Schematic of the proposed 1D photonic crystal biosensor based on a defect cavity.

equal to the sum of the thicknesses of the first and second layers, and the value $13d_d$ is the optimal thickness for the defect layer, which was obtained in the reference paper[1]. The target analyte in this research includes two types of cells: healthy cells with a refractive index of n_d =1.35 and cancerous cells from the MCF-7 line with a refractive index of n_d=1.401. The structure is designed to be symmetrical, with an equal number of periodic units on both sides of the defect layer, in order to generate a high-quality resonance mode[20].

The structure investigated in this study is based on the work presented in reference[1], and its performance is strongly dependent on the incident light angle (ϕ). In that reference, it is shown that the structure's sensitivity increases from 1020 nm/RIU at normal incidence $(\phi = 0^{\circ})$ to an optimal value of 2156 nm/RIU at an angle of φ = 85.

In the present study, this optimized structure is used as a baseline model to investigate the effect of fabrication errors on its ideal performance. However, due to fabrication limitations, the actual thickness of each layer, (d_i), is modeled as the sum of its ideal thickness, $\left(d_i^{(0)}\right)$, and a random error, $(\Delta\, d_i)$.This relationship is shown in Eq. 2:

$$d_i = d_i^{(0)} + \Delta\, d_i \tag{2}$$

The error term, $(\Delta\, d_i)$, is treated as a random variable drawn from a Normal (Gaussian) distribution, which is expressed in statistical notation as $\Delta\, d_i \sim \left(0.\sigma_i^2\right)$. Here, N signifies the Normal distribution, the 0 represents the mean of the distribution (indicating no systematic bias in the fabrication process), and σ_i^2 is the variance. The standard deviation, σ_i, dictates the width of the error distribution for each layer. It is defined by the relative fabrication error level, δ , and the layer's ideal thickness, $d_i^{(0)}$, according to the following equation:

$$\sigma_i = \delta \times d_i^{(0)} \tag{3}$$

The parameter σ_i is then used in the full mathematical expression for the Gaussian probability density function (PDF), which describes the statistical distribution of the fabrication imperfections. The probability of a layer having a specific thickness is given by Eq. 4:

$$P\left(d_i\right) = \frac{1}{\sigma_i\sqrt{2\pi}} exp\left(-\frac{\left(d_i - d_i^{(0)}\right)^2}{2\sigma_i^2}\right) \tag{4}$$

To optically analyze this structure and model the aforementioned effects, the TMM is used. In this method, the propagation of light through each dielectric layer is described by a characteristic matrix $\left(f_r^i\right)$. The total transfer matrix (F) for the entire structure is obtained by multiplying the characteristic matrices of each unique layer in sequence. Due to the random fabrication error, each layer's matrix is distinct, and the overall product for the N=5 structure is represented in Eq. 5:

$$F = \begin{bmatrix} F_{11} & F_{12} \\ F_{21} & F_{22} \end{bmatrix} = f_1^{(1)} \cdot f_2^{(1)} \cdot f_1^{(2)} \cdot f_2^{(2)} \cdots f_d \cdots f_2^{(5)} \cdot f_1^{(5)} \tag{5}$$

In this product, $f_1^{(i)}$ and $f_2^{(i)}$ represent the characteristic matrices for the first (SiO_2) and second (GaAs) layers within the i-th periodic unit, respectively, and f_d is the matrix for the central defect layer.

The characteristic matrix (f_r) for any given layer is defined by Eq. 6:

$$f_r = \begin{bmatrix} cos\varphi_r & \frac{-i}{p_r} sin\varphi_r \\ -i\, p_r sin\varphi_r & cos\varphi_r \end{bmatrix}. \quad r = 1.2.d \tag{6}$$

In the preceding relation, φ_r is the phase difference and p_r is the polarization, which were calculated in[1].

Using the elements of the total transfer matrix (F), the transmission coefficient (t) is given by Eq. 7:

$$t = \frac{2.p}{\left(F_{11} + F_{12} p_S\right) p_0 + \left(F_{21} + F_{22} p_S\right)} \tag{7}$$

In this equation, $(p_0)$and (p_s) are the optical admittances for TE-polarization in the initial medium (air) and the final medium (substrate), respectively, calculated as $p_0 = n_0\, cos\phi_0$ and $p_s = n_s\, cos\phi_s$.

Finally, the total transmittance (T), which represents the ratio of transmitted power to incident power, is calculated from the transmission coefficient (t) using Eq. 8:

$$T = \frac{p_s}{p_0}|t|^2 \tag{8}$$

To statistically evaluate the impact of fabrication errors on the sensor's performance, a numerical simulation was implemented in the MATLAB software environment. This simulation process was repeated 100 times for each fabrication error level (δ). In each iteration, a new structural instance was created with a set of random

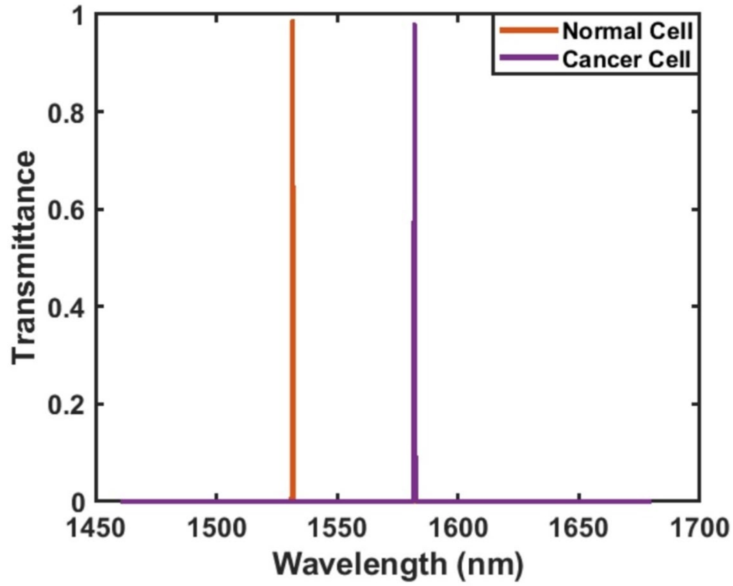

Fig. 2. Transmission peaks of healthy and cancerous cells for a zero-degree angle of incidence.

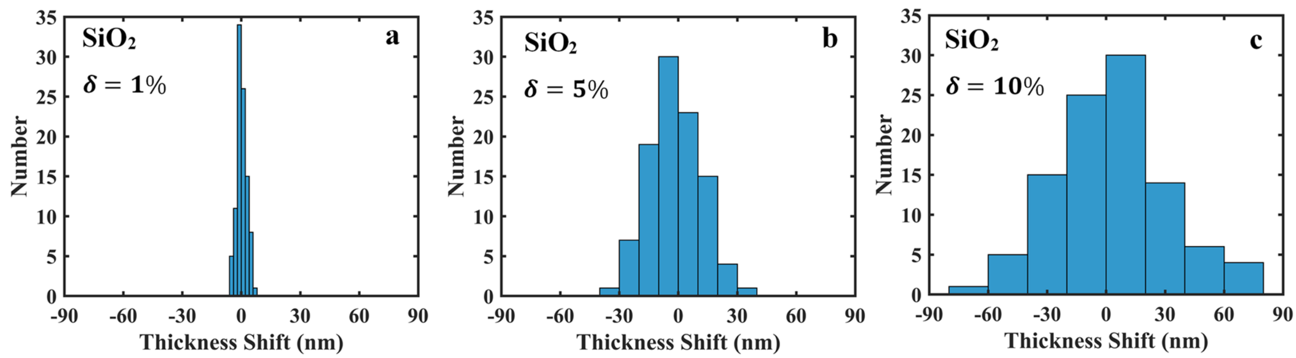

Fig. 3. Histogram of thickness deviation for the SiO_2 layer at error levels of (**a**) 1%, (**b**) 5%, and (**c**) 10%.

thicknesses, generated from the Gaussian distribution according to Eq. 2. Subsequently, its transmission spectrum and performance parameters were calculated. This range of error levels (0.5% to 10%) was specifically chosen to represent a wide spectrum of manufacturing tolerances, from high-precision fabrication techniques (below 1%) to standard and high-variation processes (5–10%) commonly reported in nanophotonic fabrication literature.

Results

To assess the impact of fabrication errors, the sensor's performance was first characterized under ideal, error-free conditions. As shown in Fig. 2, a clear distinction between healthy and cancerous cells is observed at normal incidence, with the resonance peak shifting from approximately 1705 nm to 1760 nm. This baseline provides a reference for the subsequent statistical analysis.

To investigate the impact of manufacturing imperfections, a statistical analysis was performed considering six fabrication error levels (δ): 0.5%, 1%, 2.5%, 5%, 7%, and 10%. For each level, the simulation was repeated 100 times. Fig. 3 illustrates the histogram of the resulting thickness deviations for the SiO_2 layer, confirming that as the error percentage increases, the distribution widens significantly while remaining centered around a zero mean.

The impact of these thickness variations on the sensor's optical response was then systematically investigated. We first examined the effect on the resonance peak location. A quantitative analysis of the statistical distributions shown in Fig. 4 is presented in Fig. 5. First, plots (a) and (c) analyze the broadening of the resonance peak distribution, which is quantified by its width (Wg). These plots reveal a strong linear relationship between (Wg) and the error percentage (δ) at both 0° and 85° angles, with fitted line slopes of 2.35 and 2.05, respectively. Second, plots (b) and (d) analyze the height of the fitted Gaussian curves from Fig. 4, referred to as the Peak

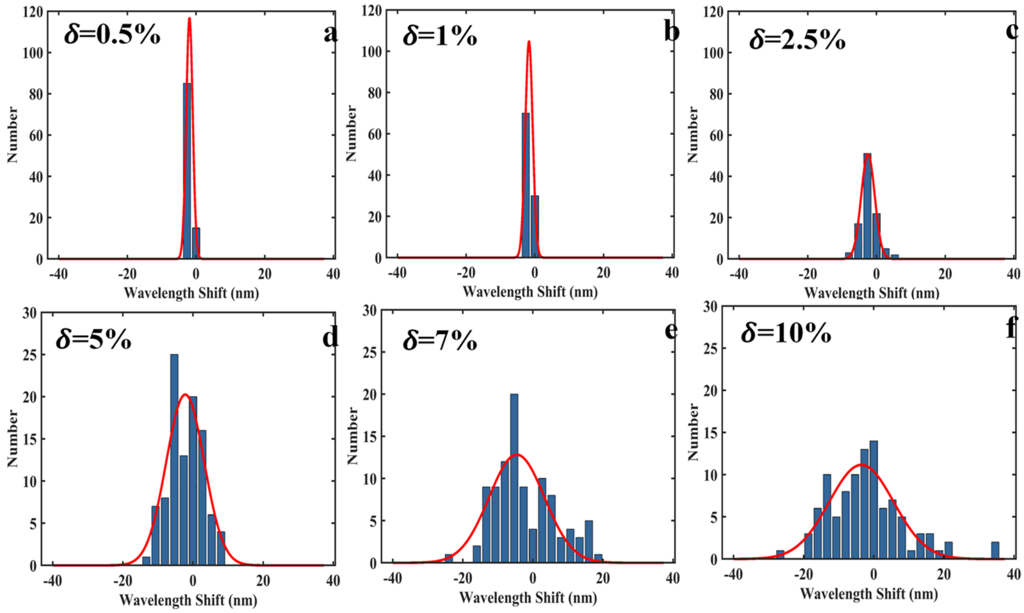

Fig. 4. Histogram of the resonance peak location (wavelength shift) for the normal cell at a zero-degree angle of incidence.

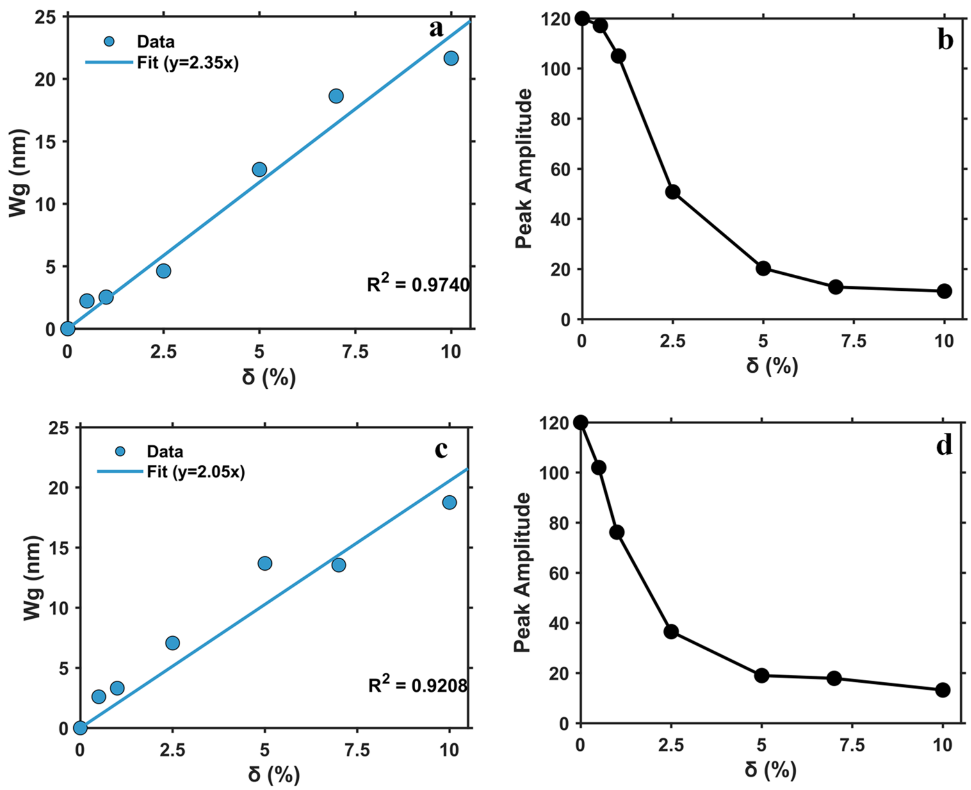

Fig. 5. Quantitative analysis of the effect of fabrication error (δ) on the statistical characteristics of the resonance peak distribution for the normal cell. plots (**a**) and (**c**) show the linear dependence of the distribution width (Wg) on the error at 0° and 85° angles, respectively. plots (**b**) and (**d**) illustrate the decreasing trend of the peak amplitude under the same conditions.

Amplitude. These plots demonstrate a sharp decreasing trend in amplitude as the fabrication error increases, confirming that the resonance peak becomes less probable and well-defined at higher error levels.

In addition to the peak's location, the quality of the resonance, characterized by its FWHM, was also analyzed. Figures 6 and 7 display the FWHM distributions for healthy and cancerous cells at the various error levels. A consistent trend of increasing dispersion in FWHM values is observed as the error percentage rises. Notably, the distributions for the 85-degree angle are visibly more stable and unimodal compared to those at normal incidence.

Finally, we evaluated how these variations in peak position and FWHM collectively impact the sensor's ultimate performance metric: its sensitivity. Figures 8 and 9 plot the sensitivity fluctuations over 100 independent simulations for three representative error levels (1%, 5%, and 10%) at incidence angles of 0° and 85°, respectively. In part (a) of each figure, the line plots show that while the mean sensitivity remains constant and equal to the ideal value, the fluctuations around this mean increase significantly with higher fabrication errors. Part (b) of each figure further illustrates this by presenting the corresponding statistical histograms, which clearly show the distribution of sensitivity values becoming progressively wider as the error level rises from 1% to 10%. Interestingly, these fluctuations allow for specific sensor instances to achieve sensitivities higher than the ideal, error-free value. The presented results show a coherent relationship. The statistical deviations in layer thickness not only lead to a dispersion in the resonance peak location (as analyzed in Figs. 4 and 5), but also manifest as an increase in the fluctuation and average value of the FWHM (Figs. 6 and 7). This general degradation in the resonance quality (corresponding to a lower Q-factor) provides a physical explanation for the observed fluctuations in the sensor's final performance metric, namely its sensitivity (Figs. 8 and 9).

Discussion

The sensor structure investigated in this study is based on the high-sensitivity design proposed by Aly and Zaky (2019)[1], which reported an ideal sensitivity of 2157 nm/RIU at an 85° incidence angle under theoretically error-free conditions. However, their work focused on an idealized model without considering the practical effects of manufacturing imperfections. The primary contribution of our research is to bridge this gap by systematically analyzing the impact of unavoidable fabrication errors on this high-sensitivity design, a crucial step for assessing its real-world viability.

To provide a quantitative assessment of the impact of fabrication error and to validate the claim of robustness at a high incidence angle, the key statistical parameters of the sensor's performance are summarized in Table 1. This data was extracted from the 100 simulation iterations for each error level. As the table indicates, while the mean sensitivity value remains constant and close to the ideal value at both angles, the Standard Deviation of the sensitivity at the 85° angle is significantly lower than at the 0° angle (especially at high error levels such as 10%). This finding quantitatively confirms that the 85° angle, in addition to providing higher sensitivity, also exhibits substantially better stability and robustness against the statistical fluctuations caused by fabrication errors.

To precisely situate the novelty of this research, Table 2 compares the present work with key studies that have analyzed fabrication errors in photonic crystals. Unlike the foundational work[1], which focused on an ideal (error-free) sensor, these studies investigate the effects of real manufacturing imperfections.

As summarized in Table 2, these studies have either addressed different structures (such as 2D-PC sensors [Fallahi et al.; Dell'Olio et al.][61,69] or (1D-PC BSW sensors)[54], or have assessed different error parameters (such as hole radius errors).

To contextualize the robustness of the sensor, a comparison can be made with the other works introduced in Table 2. Anopchenko et al.[54] performed a similar analysis on Bloch Surface Wave (BSW) sensors. Our results (particularly the histograms in Fig. 4, showing the statistical distribution of the resonance wavelength) are conceptually similar to Fig. 3 of [54], where they presented histograms of the BSW resonance angle distribution resulting from a $\pm 3\%$ thickness disorder[54]. Anopchenko et al. found a standard deviation of 0.17 degrees in the resonance angle and concluded that their sensor was "sufficiently robust"[54]. For instance, Fallahi et al.[61] also performed a statistical evaluation of 'sensitivity fluctuations' at various 'hole radius' error levels, which is conceptually similar to the analysis in our Fig. 8. Likewise, Dell'Olio et al.[69]. demonstrated how hole radius errors impact the Q-factor in polymer filters. A key distinction is that the analysis by Anopchenko et al.[54] was supported by experimental measurements, whereas this study (similar to [61] and [69]) provides a purely numerical framework for evaluating the robustness of a high-sensitivity, cavity-based 1D-PC sensor.

Conclusion

In this research, the impact of fabrication errors (Fab-errors) on the performance of a 1D-PC biosensor, optimized for cancer detection, was investigated. Using the TMM and a comprehensive statistical simulation, the effects of random deviations in layer thickness were analyzed at various error levels (δ) and at two incidence angles (0° and 85°).

The results indicated that as the fabrication error percentage increases, the resonance peak position and the FWHM deviate from their ideal values, and their statistical fluctuations increase. The key finding of this study is that the 85° incidence angle—previously optimized for high sensitivity—demonstrates significantly higher resistance and robustness against fabrication errors compared to normal incidence (0°). Furthermore, the statistical analysis revealed that some instances with errors could, surprisingly, achieve sensitivities higher than the ideal (error-free) value. These findings provide a quantitative framework for sensor designers to evaluate the trade-off between fabrication tolerances and device performance stability. More importantly, this study shows that the selection of the optimal incidence angle (85°) is crucial not only for achieving maximum sensitivity but also as a smart choice to ensure sensor stability against fabrication imperfections.

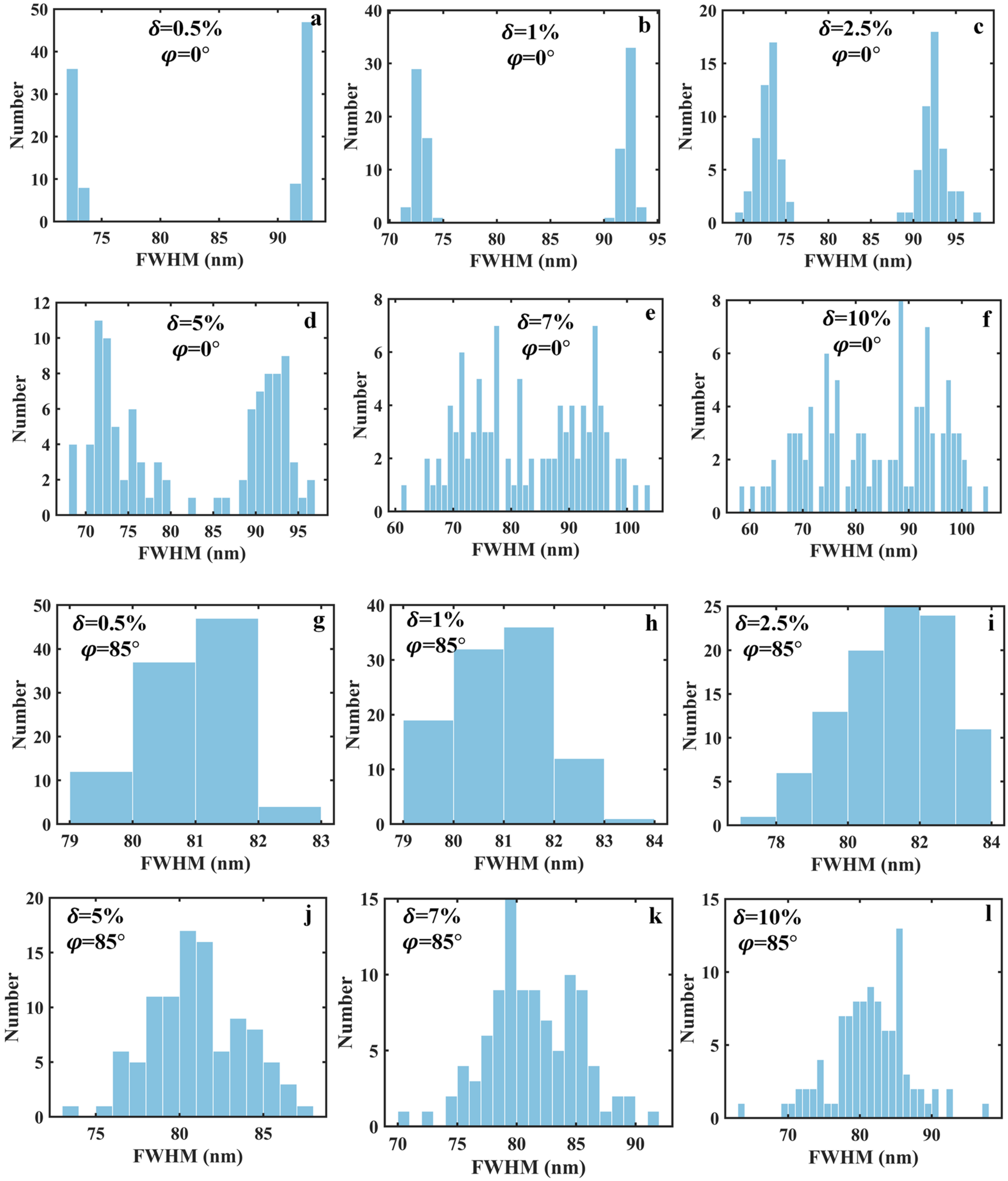

Fig. 6. Histogram of FWHM values for the healthy cell's resonance peak at different levels of fabrication error (δ). the top row (**a**-**f**) shows the results for a normal incidence angle $\left(\phi = 0^{\circ}\right)$, while the bottom row (**g**-**l**) shows the results for an 85-degree incidence angle $\left(\phi = 85^{\circ}\right)$.

The scope of the present study is primarily limited to a numerical simulation framework. Therefore, an experimental validation of these statistical findings would be a valuable extension of this work. Additionally, while this study analyzed key optical parameters (sensitivity and FWHM), investigating the impact of fabrication errors on other performance metrics—such as response time and specificity, which are beyond the scope of this

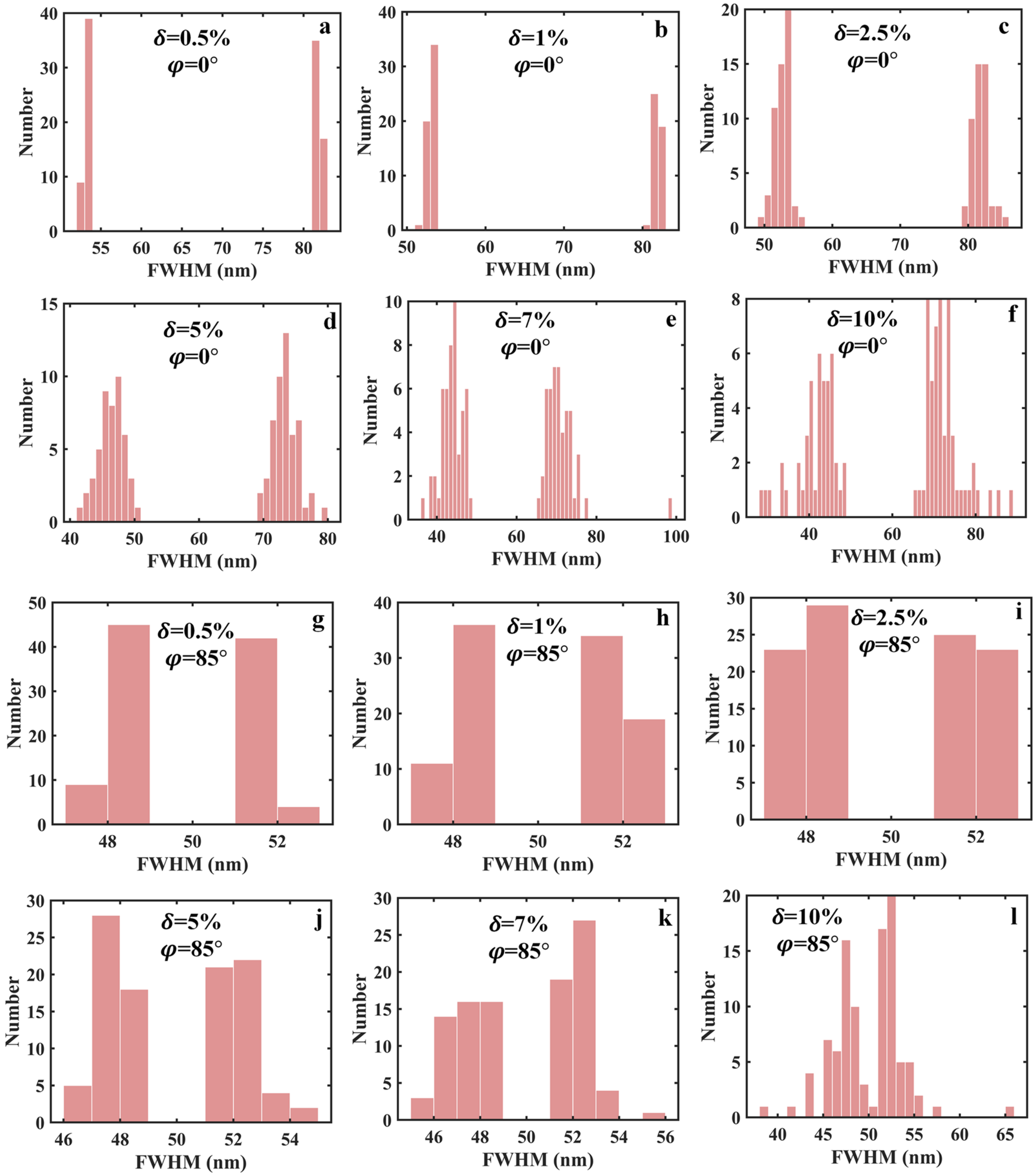

Fig. 7. Histogram of FWHM values for the cancerous cell's resonance peak at different levels of fabrication error (δ). the top row (**a**-**f**) shows the results for a normal incidence angle $\left(\phi = 0^{\circ}\right)$, while the bottom row (**g**-**l**) shows the results for an 85-degree incidence angle $\left(\phi = 85^{\circ}\right)$.

purely optical model—presents an important avenue for future research. It is recommended that future work investigates the physical origin of the increased sensitivity observed in some error-prone instances, as well as the generalizability of these findings to other photonic structures (such as 2D-PCs).

The authors gratefully acknowledge the support of the Department of Physics, Shiraz University of Technology, for providing access to the high-performance computing systems that made the numerical simulations in this study possible.

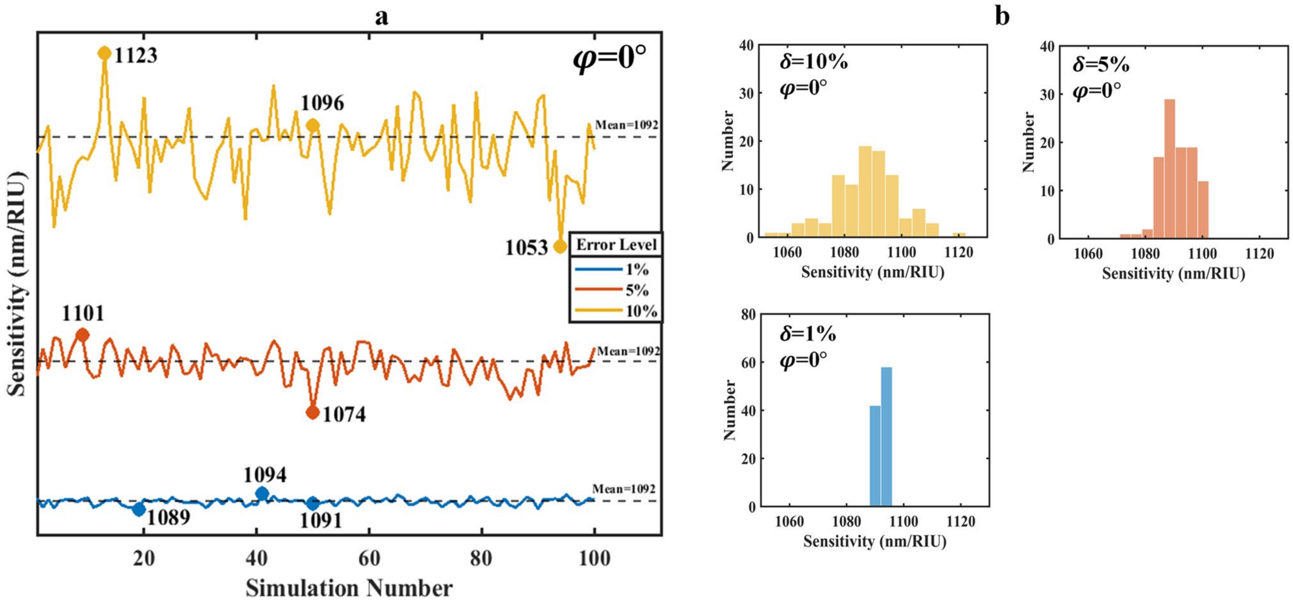

Fig. 8. Sensor sensitivity at an incidence angle of $\left(\phi = 0^{\circ}\right)$. (**a**) Fluctuation of sensitivity values over 100 independent simulations for three fabrication error levels. (**b**) Corresponding statistical histograms showing the distribution of sensitivity values for each error level.

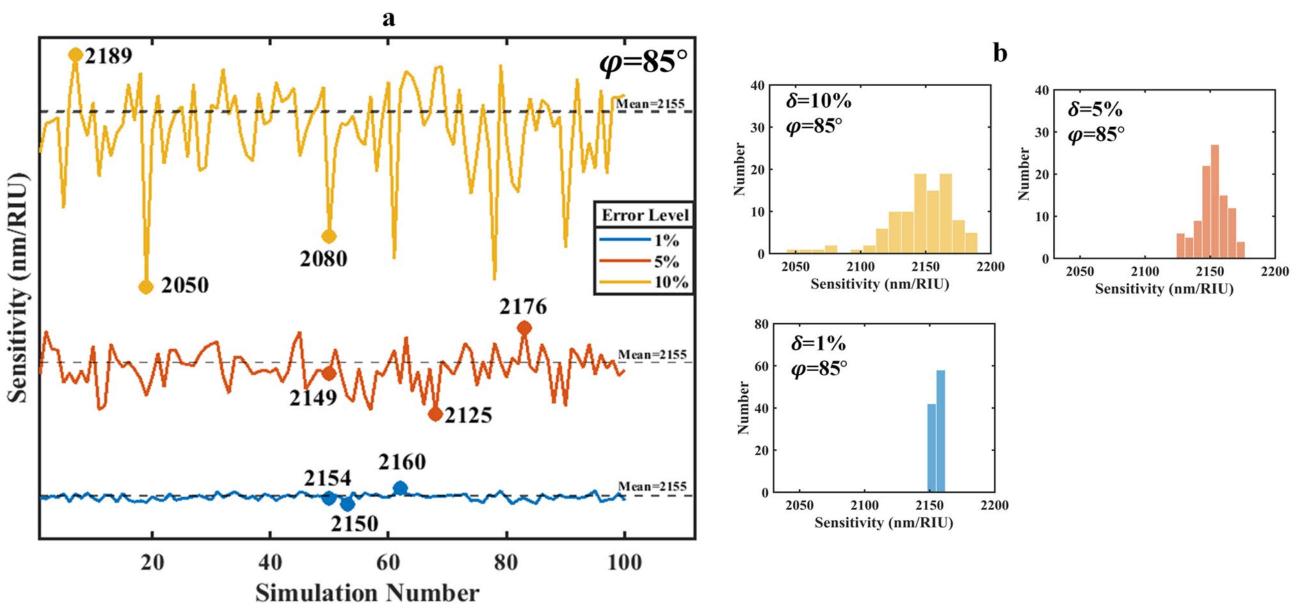

Fig. 9. Sensor sensitivity at an incidence angle of $\left(\phi = 85^{\circ}\right)$. (**a**) Fluctuation of sensitivity values over 100 independent simulations for three fabrication error levels. (**b**) Corresponding statistical histograms showing the distribution of sensitivity values for each error level.

Incidence Angle (ϕ (	Error Level (δ)	Mean Sensitivity (nm/RIU)	Std. Dev. Sensitivity (nm/RIU)	Mean FWHM (Healthy) (nm)	Std.Dev. FWHM (Healthy) (nm)	Mean FWHM (Cancer) (nm)	Std. Dev. FWHM (Cancer) (nm)
0°	1%	1092.4	0.6	81.6	7.8	62.8	9.3
	5%	1092.4	1.9	82.7	9.7	61.8	11.3
	10%	1092.1	3.9	84.4	12.1	62.0	13.6
85°	1%	2155.6	1.1	81.2	0.9	49.9	1.1
	5%	2155.6	2.5	81.5	2.5	50.2	1.8
	10%	2155.1	4.8	82.1	3.5	50.7	3.1

Table 1. Statistical summary of sensor performance under fabrication error, based on 100 iterations per error level.

Reference	Structure	Error Parameter	Key Finding on Error Impact
Anopchenko et al.[54]	1D-PC (BSW Sensor)	Layer Thickness ($\pm 3\% Error$)	Resonance angle stability (σ_θ =0.17 $^\circ$ Std. dev.) concluded as "sufficiently robust".
Fallahi et al.[61]	2D-PC (Ring Resonator)	Hole Radius (up to 15% Error)	High sensitivity fluctuation; sensitivity nearly doubled (from 830 to $\approx$ 1570 nm/RIU) at 15% Error
Dell'Olio et al.[69]	2D-PC (Polymer Filter)	Hole Radius/Position	Q-factor degradation; tolerance limit for 70% production yield set atproduction yield set at $\pm$ 5nm in Hole Radius
This Work	1D-PC (Cavity)	Layer Thickness	High sensitivity stability (mean $\approx$ 2155 nm/RIU); the 85 $^\circ$ angle provided superior robustness against error.

Table 2. Comparison of the fabrication error analysis in this work with related studies.

Data availability

The datasets generated and analysed during the current study are available from the corresponding author on reasonable request.

Received: 26 August 2025; Accepted: 31 January 2026
Published online: 07 February 2026

References

1. Aly, A. H. & Zaky, Z. A. Ultra-sensitive photonic crystal cancer cells sensor with a high-quality factor. *Cryogenics* **104**, 102991 (2019).
2. Zajnulina, M. Advances of Artificial Intelligence in Classical and Novel Spectroscopy-Based Approaches for Cancer Diagnostics. A Review [Internet]. arXiv; [cited 2025 Jul 11]. (2022). Available from: http://arxiv.org/abs/2208.04008
3. Khani, S. & Hayati, M. Optical biosensors using plasmonic and photonic crystal band-gap structures for the detection of basal cell cancer. *Sci. Rep.* **12** (1), 5246 (2022).
4. Talreja, R. K. et al. Challenges in Lab-to-Clinic translation of 5th/6th generation intelligent nanomaterial-enabled biosensors. *ECS Sens. Plus*. **3** (4), 041602 (2024).
5. Chaudhary, V. et al. Nose-on-Chip nanobiosensors for early detection of lung cancer breath biomarkers. *ACS Sens.* **9** (9), 4469–4494 (2024).
6. Taha, B. A. et al. Advancing cancer diagnostics through multifaceted optical biosensors supported by nanomaterials and artificial intelligence: A panoramic outlook. *Microchem J.* **205**, 111307 (2024).
7. Singhal, N. et al. A deep learning system for prostate cancer diagnosis and grading in whole slide images of core needle biopsies. *Sci. Rep.* **12** (1), 3383 (2022).
8. De Miguel Pérez, D. et al. Extracellular vesicle-miRNAs as liquid biopsy biomarkers for disease identification and prognosis in metastatic colorectal cancer patients. *Sci. Rep.* **10** (1), 3974 (2020).
9. Desroches, J. et al. A new method using Raman spectroscopy for in vivo targeted brain cancer tissue biopsy. *Sci. Rep.* **8** (1), 1792 (2018).
10. Taha, B. A. et al. Multifunctional nanophotonic photoacoustic biosensors: a new era in molecular imaging–guided deep-tissue cancer monitoring. Methods [Internet]. [cited 2025 Nov 10]; (2025). Available from: https://www.sciencedirect.com/science/article/pii/S1046202325001458
11. Taha, B. A. et al. Nanophotonic catheters: A lens into the body for biosensing and biomedical imaging. *Appl. Mater. Today*. **38**, 102229 (2024).
12. Taha, B. A. et al. Nanostructured photonics probes: a transformative approach in neurotherapeutics and brain circuitry. *Neuroscience* **562**, 106–124 (2024).
13. Saklani, S. et al. Nanomaterials-integrated electrochemical biosensors as pioneering solutions for zoonotic disease diagnosis. *J. Electrochem. Soc.* **171** (8), 087502 (2024).
14. Chaudhary, V., Lucky, L., Sable, H. & Bhalla, N. Interdisciplinary approach to Monkeypox prevention: integrating nanobiosensors, nanovaccines, artificial intelligence, visual arts, and social sciences. *Small Struct.* ;**6** (7), 2400647 (2025).
15. Chaudhary, V., Sable, H., Kumar, M., Prakash, C. & Sonu, S. Dynamic landscape of chemiresistive breathomic nanosensors based on fifth-generation chips for complex disease diagnosis and healthcare monitoring. Appl Phys Rev [Internet]. [cited 2025 Dec 11];12(4). (2025). Available from: https://pubs.aip.org/aip/apr/article/12/4/041311/3371043
16. Nair, R. V. & Vijaya, R. Photonic crystal sensors: an overview. *Prog Quantum Electron.* **34** (3), 89–134 (2010).
17. Chen, K. M. et al. SiO 2/TiO 2 omnidirectional reflector and microcavity resonator via the sol-gel method. *Appl. Phys. Lett.* **75** (24), 3805–3807 (1999).

18. Lee, H. Y., Makino, H., Yao, T. & Tanaka, A. Si-based omnidirectional reflector and transmission filter optimized at a wavelength of 1.55 μm. *Appl. Phys. Lett.* **81** (24), 4502–4504 (2002).
19. Patrini, M. et al. Optical response of one-dimensional (Si/SiO 2) m photonic crystals. *J. Appl. Phys.* **92** (4), 1816–1820 (2002).
20. Fallahi, V., Kordrostami, Z. & Hosseini, M. Sensitivity and quality factor improvement of photonic crystal sensors by geometrical optimization of waveguides and micro-ring resonators combination. *Sci. Rep.* **14** (1), 2001 (2024).
21. Aly, A. H. et al. Ultra-high sensitive cancerous cells detection and sensing capabilities of photonic biosensor. *Sci. Rep.* **13** (1), 19524 (2023).
22. Meade, R. D. V., Johnson, S. G. & Winn, J. N. Photonic Crystals: Molding the Flow of Light - Second Edition [Internet]. Princeton University Press; [cited 2025 Jul 11]. Available from: https://www.degruyter.com/document/doi/ (2008). https://doi.org/10.1515/9781400828241/html
23. Aly, A. H. et al. Detection of reproductive hormones in females by using 1D photonic crystal-based simple reconfigurable biosensing design. *Crystals* **11** (12), 1533 (2021).
24. Yablonovitch, E. Inhibited spontaneous emission in Solid-State physics and electronics. *Phys. Rev. Lett.* **58** (20), 2059–2062 (1987).
25. Hajshahvaladi, L., Kaatuzian, H., Moghaddasi, M. & Danaie, M. Hybridization of surface plasmons and photonic crystal resonators for high-sensitivity and high-resolution sensing applications. *Sci. Rep.* **12** (1), 21292 (2022).
26. Frascella, F. et al. A fluorescent one-dimensional photonic crystal for label-free biosensing based on Bloch surface waves. *Sensors* **13** (2), 2011–2022 (2013).
27. Bonifacio, L. D. et al. Towards the photonic nose: A novel platform for molecule and bacteria identification. *Adv. Mater.* **22** (12), 1351–1354 (2010).
28. Zhao, Y., Zhao, X. & Gu, Z. Photonic crystals in bioassays. *Adv. Funct. Mater.* **20** (18), 2970–2988 (2010).
29. Ayyub, O. B., Ibrahim, M. B., Briber, R. M. & Kofinas, P. Self-assembled block copolymer photonic crystal for selective Fructose detection. *Biosens. Bioelectron.* **46**, 124–129 (2013).
30. Fallahi, V., Kordrostami, Z. & Hosseini, M. A solution for detection of ethanol and methanol with overlapping refractive indexes based on photonic crystal ring resonator optical sensors. *IEEE Sens. J.* **23** (7), 6791–6798 (2023).
31. Mehta, K. K. et al. High-Q CMOS-integrated photonic crystal microcavity devices. *Sci. Rep.* **4** (1), 4077 (2014).
32. Abe, S., Joichi, T., Uekusa, K., Hara, H. & Masuda, S. Photonic integration based on a ferroelectric thin-film platform. *Sci. Rep.* **9** (1), 16548 (2019).
33. Wang, F. et al. Nanoscale on-chip all-optical logic parity checker in integrated plasmonic circuits in optical communication range. *Sci. Rep.* **6** (1), 24433 (2016).
34. Shi, J. et al. Photonic crystal and quasi-crystals providing simultaneous light coupling and beam splitting within a low refractive-index slab waveguide. *Sci. Rep.* **7** (1), 1812 (2017).
35. Fan, X. et al. Sensitive optical biosensors for unlabeled targets: A review. *Anal. Chim. Acta*. **620** (1–2), 8–26 (2008).
36. John, S. Strong localization of photons in certain disordered dielectric superlattices. *Phys. Rev. Lett.* **58** (23), 2486–2489 (1987).
37. Aly, A. H. et al. Study on a one-dimensional defective photonic crystal suitable for organic compound sensing applications. *RSC Adv.* **11** (52), 32973–32980 (2021).
38. Gandhi, S., Awasthi, S. K. & Aly, A. H. Biophotonic sensor design using a 1D defective annular photonic crystal for the detection of creatinine concentration in blood serum. *RSC Adv.* **11** (43), 26655–26665 (2021).
39. Efimov, I. M., Vanyushkin, N. A., Gevorgyan, A. H. & Golik, S. S. Optical biosensor based on a photonic crystal with a defective layer designed to determine the concentration of SARS-CoV-2 in water. *Phys. Scr.* **97** (5), 055506 (2022).
40. Sayed, H., Ahmed, A. M., Hajjiah, A., Abdelkawy, M. A. & Aly, A. H. Highly sensitive salinity sensing using annular one-dimensional photonic crystals. *Sci. Rep.* **15** (1), 18337 (2025).
41. Shaban, M., Ahmed, A. M., Abdel-Rahman, E. & Hamdy, H. Tunability and sensing properties of Plasmonic/1D photonic crystal. *Sci. Rep.* **7** (1), 41983 (2017).
42. Lv, X. et al. Research progress in Preparation and application of photonic crystals. *Chin. J. Mech. Eng.* **36** (1), 39 (2023).
43. Gonzalez-Valencia, E., Villar, I. D. & Torres, P. Novel Bloch wave excitation platform based on few-layer photonic crystal deposited on D-shaped optical fiber. *Sci. Rep.* **11** (1), 11266 (2021).
44. Çetinkaya, Ç. et al. Enhancement of color and photovoltaic performance of semi-transparent organic solar cell via fine-tuned 1D photonic crystal. *Sci. Rep.* **12** (1), 19400 (2022).
45. Maher, M. A., Aly, A. H., Esmail, M. S. & El-Ghany, S. E. S. A. Maximizing temperature sensitivity in a one-dimensional photonic crystal thermal sensor. *Sci. Rep.* **15** (1), 4105 (2025).
46. Sayed, H., Ahmed, A. M., Hajjiah, A., Abdelkawy, M. A. & Aly, A. H. Optimization of amorphous silicon solar cells through photonic crystals for enhanced optical properties. *Sci. Rep.* **15** (1), 16529 (2025).
47. González, L. E. et al. Experimental realisation of tunable ferroelectric/superconductor (BTO/YBCO) N/STO 1D photonic crystals in the whole visible spectrum. *Sci. Rep.* **10** (1), 13083 (2020).
48. Bellessa, J. et al. Eu 3+-doped microcavities fabricated by sol–gel process. *Appl. Phys. Lett.* **79** (14), 2142–2144 (2001).
49. Goyal, A. K., Divyanshu, D. & Massoud, Y. Excitation of optical Tamm state for photonic spin hall enhancement. *Sci. Rep.* **14** (1), 175 (2024).
50. Reece, P. J., Gal, M., Lerondel, G., Tan, H. H. & Jagadish, C. Light emission from 1D silicon photonic crystals containing erbium. In: Optoelectronic integration on silicon [Internet]. SPIE; [cited 2025 Jul 11]. pp. 126–34. Available from: https://www.spiedigitallibrary.org/conference-proceedings-of-spie/5357/0000/Light-emission-from-1D-silicon-photonic-crystals-containing-erbium/ (2004). https://doi.org/10.1117/12.525966.short
51. Biswas, U., Nayak, C. & Rakshit, J. K. Fabrication techniques and applications of two-dimensional photonic crystal: history and the present status. Opt Eng [Internet]. Dec 23 [cited 2025 Jul 3];62(01). Available from: https://www.spiedigitallibrary.org/journals/optical-engineering/volume-62/issue-01/010901/Fabrication-techniques-and-applications-of-two-dimensional-photonic-crystal/ (2022). https://doi.org/10.1117/1.OE.62.1.010901.full
52. Ramirez-Gutierrez, C. F., Martinez-Hernandez, H. D., Lujan-Cabrera, I. A. & Rodriguez-García, M. E. Design, fabrication, and optical characterization of one-dimensional photonic crystals based on porous silicon assisted by in-situ photoacoustics. *Sci. Rep.* **9** (1), 14732 (2019).
53. Li, L., Schröder, T., Chen, E. H., Bakhru, H. & Englund, D. One-dimensional photonic crystal cavities in single-crystal diamond. *Photonics Nanostruct. - Fundam Appl.* **15**, 130–136 (2015).
54. Anopchenko, A. et al. Effect of thickness disorder on the performance of photonic crystal surface wave sensors. *Opt. Express*. **24** (7), 7728–7742 (2016).
55. Tikhodeev, S. G. et al. Influence of disorder on a Bragg microcavity. *J. Opt. Soc. Am. B*. **38** (1), 139–150 (2020).
56. Bragheri, F., Faccio, D., Romagnoli, M., Krauss, T. & Roberts, J. Effects of random and systematic perturbations in a one-dimensional photonic crystal wavelength converter. *Phys. Rev. E*. **70** (1), 017601 (2004).
57. García, P. D., Javadi, A., Thyrrestrup, H. & Lodahl, P. Quantifying the intrinsic amount of fabrication disorder in photonic-crystal waveguides from optical far-field intensity measurements. Appl Phys Lett [Internet]. [cited 2025 Nov 10];102(3). (2013). Available from: https://pubs.aip.org/aip/apl/article/102/3/031101/384772
58. Bommer, S. P. et al. Transfer printing micro-assembly of silicon photonic crystal cavity arrays: beating the fabrication tolerance limit. *Nat. Commun.* **16** (1), 5994 (2025).
59. Srinivasan, K., Barclay, P. E. & Painter, O. Fabrication-tolerant high quality factor photonic crystal microcavities. *Opt. Express*. **12** (7), 1458–1463 (2004).

60. Caballero, L. E. P., Cano, J. P. V., Guimaraes, P. S. & Neto, O. P. V. Effect of structural disorder on photonic crystal logic gates. *IEEE Photonics J.* **9** (5), 1–15 (2017).
61. Fallahi, V., Hosseini, M. & Kordrostami, Z. Analysis of Manufacturing Process Errors on the Functionality of Photonic Crystal Sensors. IEEE Sens J [Internet]. [cited 2025 Nov 10]; (2025). Available from: https://ieeexplore.ieee.org/abstract/document/11087471/
62. Parvin, T., Ahmed, K., Alatwi, A. M. & Rashed, A. N. Z. Differential optical absorption spectroscopy-based refractive index sensor for cancer cell detection. *Opt. Rev.* **28** (1), 134–143 (2021).
63. Liu, P. Y. et al. Cell refractive index for cell biology and disease diagnosis: past, present and future. *Lab. Chip*. **16** (4), 634–644 (2016).
64. Wang, Z., Popescu, G., Tangella, K. V. & Balla, A. Tissue refractive index as marker of disease. *J. Biomed. Opt.* **16** (11), 1 (2011).
65. Bista, R. K. et al. Quantification of nanoscale nuclear refractive index changes during the cell cycle. *J. Biomed. Opt.* **16** (7), 070503 (2011).
66. Fallahi, V., Kordrostami, Z. & Hosseini, M. Cancer detection by photonic crystal optical biosensors: effect of hexagonal micro ring resonator design. *Mater. Sci. Semicond. Process.* **174**, 108188 (2024).
67. Fallahi, V., Hosseini, M. & Kordrostami, Z. Optimization of highly sensitive three-layer photonic crystal fiber sensor based on plasmonic. *Phys. Scr.* **99** (10), 105577 (2024).
68. Segura, D., Vega, D., Cardador, D. & Rodriguez, A. Effect of fabrication tolerances in macroporous silicon photonic crystals. *Sens. Actuators Phys.* **264**, 172–179 (2017).
69. Dell'Olio, F., Ciminelli, C., Conteduca, D. & Armenise, M. N. Effect of fabrication tolerances on the performance of two-dimensional polymer photonic crystal channel drop filters: a theoretical investigation based on the finite element method. *Opt. Eng.* **52** (9), 097104–097104 (2013).

Acknowledgements
The authors gratefully acknowledge the support of the Department of Physics, Shiraz University of Technology, for providing access to the high-performance computing systems that made the numerical simulations in this study possible.

Author contributions
S. A. Mohammadi and M. Hosseini wrote the main manuscript text and A. Mohammadi prepared figures. All authors reviewed the manuscript.

Funding
The authors received no specific funding for this work.

Declarations

Competing interests
The authors declare no competing interests.

Ethical approval
This article does not contain any studies with human participants or animals performed by any of the authors.

Additional information

Correspondence and requests for materials should be addressed to M.H.